Phase Separation and Pair Condensation in a Spin-Imbalanced 2D Fermi Gas

Debayan Mitra,* Peter T. Brown, Peter Schauß, Stanimir S. Kondov, and Waseem S. Bakr
Department of Physics, Princeton University, Princeton, New Jersey 08544, USA
(Received 19 April 2016; revised manuscript received 30 June 2016; published 24 August 2016)

We study a two-component quasi-two-dimensional Fermi gas with imbalanced spin populations. We probe the gas at different interaction strengths and polarizations by measuring the density of each spin component in the trap and the pair momentum distribution after time of flight. For a wide range of experimental parameters, we observe in-trap phase separation characterized by the appearance of a spin-balanced core surrounded by a polarized gas. Our momentum space measurements indicate pair condensation in the imbalanced gas even for large polarizations where phase separation vanishes, pointing to the presence of a polarized pair condensate. Our observation of zero momentum pair condensates in 2D spin-imbalanced gases opens the way to explorations of more exotic superfluid phases that occupy a large part of the phase diagram in lower dimensions.

DOI: 10.1103/PhysRevLett.117.093601

Fermionic superfluids described by standard Bardeen-Cooper-Schrieffer theory are momentum-space condensates of Cooper pairs of opposite spins. Imbalancing the chemical potentials of the two spin species disrupts the Cooper pairing mechanism and can give rise to many interesting scenarios. For a small difference in the chemical potentials, the Fermi gas remains a spin-balanced superfluid. As the chemical potential imbalance is increased, it eventually becomes comparable to the superfluid gap. At this point, known as the Clogston-Chandrasekhar limit [1], the gas becomes polarized but superfluidity may persist due to the presence of exotic superfluid phases such as the Sarma [2] or FFLO phase [3,4]. Eventually, for large enough chemical potential difference, superfluidity is completely destroyed. The stability of some exotic superfluid phases like FFLO is greatly enhanced by lowering the dimensionality of the gas [5,6].

The search for exotic superfluids motivates our study of spin-imbalanced atomic Fermi gases in two dimensions. In addition, the 2D case becomes particularly interesting in the case of strong interactions [7–10]. In an atomic gas, Feshbach resonances enable tuning the interactions over a wide range and studying the effect of chemical potential imbalance beyond the described weak coupling BCS limit. Unlike the 1D case, exact solutions do not exist, and mean field models that do well in three dimensions fail in two dimensions due to the enhanced role of quantum fluctuations [11,12].

Spin-imbalanced Fermi gases have been extensively studied both theoretically [13–17] and experimentally [18]. Experiments in three dimensions have observed vortex lattices in spin-imbalanced superfluids [19] as well as phase separation between the superfluid and normal phases in the trapped gas [20–22]. Subsequent experiments quantitatively mapped out the phase diagram of the 3D gas [23,24] and measured the equation of state of the imbalanced gas [25,26]. In one dimension, phase separation was also observed, displaying an inverted phase profile in the trap compared to three dimensions [27]. Recent experiments have started to explore 2D Fermi gases [28–37], mostly focusing on the spin-balanced case, where pair condensation has been observed [38] and the BKT nature of the transition to the superfluid state was explored [39,40]. The properties of the polaron were characterized in experiments studying the extreme imbalance limit [41]. A noninteracting polaron model was found to be adequate for describing high-polarization 2D Fermi gases in the BCS regime and a spin-balanced central core was observed on the BEC side [42].

Our experiments measure the density profile of a single-layer 2D gas, revealing a spin-balanced core at low to intermediate polarizations. We explore the stability of this spin-balanced core for varying chemical potential, chemical potential difference between the spin species, and interaction strengths across the Feshbach resonance. On the BEC side of the 3D unitarity point, measurement of the momentum distribution in time of flight reveals a pair condensate. Condensation is observed past the disappearance of phase separation, implying that unpaired majority atoms become dissolved in the condensate, forming a polarized condensate.

We realize a strongly interacting Fermi gas using a mixture of the lowest two hyperfine ground states of ^{6}Li, $|1\rangle$ and $|2\rangle$. The global spin imbalance P is defined as $P = [(N_\uparrow - N_\downarrow)/(N_\uparrow + N_\downarrow)]$, where $N_\uparrow$ is the population in the majority state ($|1\rangle$), and $N_\downarrow$ is the population in the minority state ($|2\rangle$). P can be varied continuously from a balanced to an almost completely polarized gas. The interaction strength is varied by tuning the s-wave scattering length using a broad Feshbach resonance centered at 832 G.

To create the ultracold sample, we load atoms from a magneto-optical trap into a 1 mK deep crossed optical dipole trap. Starting from a spin-balanced mixture, the spin populations are imbalanced by transferring a variable fraction of the $|2\rangle$ atoms into a third hyperfine state $|3\rangle$, employing a diabatic Landau-Zener sweep [43]. The $|3\rangle$ atoms are then

removed from the trap with a resonant light pulse before proceeding with all-optical evaporation at the Feshbach resonance. The imbalanced mixture is transferred to a highly anisotropic optical trap with aspect ratio $\omega_x:\omega_y:\omega_z = 1:3:30$. The large confinement anisotropy allows efficient transfer into a single well of a 1D optical lattice with a 12 μm lattice spacing formed by two 532 nm laser beams intersecting at a shallow angle that can be dynamically adjusted to change the lattice spacing [Fig. 1(a)]. In the plane, the atoms are confined by a vertical 1070 nm beam with a 100 μm waist. Subsequently, the Feshbach field is adjusted to set the interaction strength in the gas and the lattice spacing is decreased to 3.5 μm, resulting in trapping frequencies $(\omega_x, \omega_y, \omega_z) = 2\pi(124\text{ Hz}, 147\text{ Hz}, 22.5\text{ kHz})$. To ensure that the gas is in the 2D regime the chemical potential of the majority atoms, $\mu_{0\uparrow}$, is kept below the axial vibrational level spacing $\hbar\omega_z$. This condition is satisfied by keeping the majority atom number fixed to $\sim 9 \times 10^3$, resulting in $\mu_{0\uparrow}/\hbar\omega_z < 0.7$ over the full parameter regime. Our ability to load a single layer is confirmed by taking an absorption image of the cloud on-edge through an auxiliary imaging system. Example images of single and multiple loaded layers are shown in Fig. 1(b).

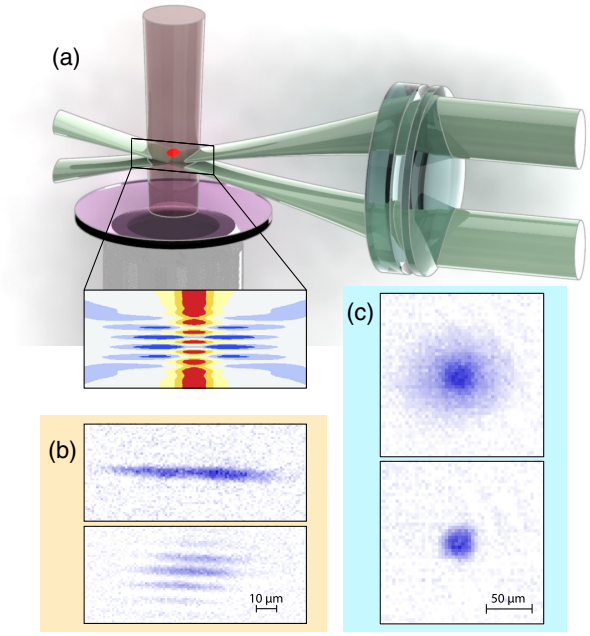

FIG. 1. Experimental setup. (a) A 1D optical lattice is formed at the intersection of two interfering blue-detuned beams (green), providing axial confinement. The lattice spacing can be dynamically tuned by changing the angle between the beams. The atoms are radially confined by a red-detuned beam (brown) in the vertical direction. A high-NA objective (gray) is used to image the in-plane density distribution. The inset shows a section of the optical potential with color scale from red (attractive) to blue (repulsive). (b) Side absorption images illustrating our capability to load and resolve single (above) and multiple pancakes (below) after adiabatically increasing the lattice spacing to ~ 12 μm. (c) *In situ* absorption images of majority (above) and minority (below) clouds along the vertical direction at 755 G and polarization $P = 0.6$.

We take absorption images of the minority and majority density distributions using two consecutive resonant pulses to obtain the optical density (OD) of the sample [Fig. 1(c) and Ref. [43]], which is directly proportional to the two-dimensional atomic density. The minority image is always taken first, although we have checked that the effect of heating due to the first imaging pulse is not measurable within our experimental noise.

An *in situ* image reveals the density of each spin component $n_\uparrow(r)$ and $n_\downarrow(r)$ and the local polarization $p(r) = [(n_\uparrow - n_\downarrow)/(n_\uparrow + n_\downarrow)]$ after azimuthally averaging over elliptical contour lines. Figures 2(a)–2(c) show *in situ* density profiles for three different polarizations at 780 G. For all shown polarizations we observe a dip in the center of the difference OD. For $P = 0.25$ the central polarization is consistent with zero, while for $P = 0.75$ we observe a clear difference in central density for minority and majority components. These spatially varying profiles can be understood in the local density approximation. While the difference between the chemical potentials of the two species remains fixed throughout the trap, the average chemical potential is scanned by the trap. Thus one can expect shells of coexisting phases in the trap. The insets in Fig. 2 show an example of such structure where a balanced phase exists in the trap center, surrounded by a partially polarized gas which is, in turn, enclosed by a shell of fully polarized gas of majority atoms. A Fermi-Dirac fit to the tail of the radial majority density profile yields $T/T_F = k_B T/\mu_{0\uparrow} = 0.18(5)$ independent of polarization, and only weakly dependent on the Feshbach field [43]. We note that this definition of T_F deviates from the definition via the central density (T_F^0) used elsewhere [38]. For our balanced data on the BEC side, we get $T/T_F^0 = 0.10(3)$ [43].

The existence of a spin-balanced core strongly suggests the presence of a condensate in that region of the trap. To probe pair condensation more directly, we measured the density of the minority component after a 3 ms time of flight. Unlike Ref. [38], we did not perform a rapid ramp to the BEC side, but simply released the gas from the trap. The expansion along the axial direction of the 2D gas leads to a rapid reduction of the density of the gas during time of flight, and the pair center-of-mass momentum distribution is not significantly affected by scattering events. We observe bimodal distributions that fit well to the sum of two Gaussian profiles. Examples are shown in Figs. 2(d)–2(f) corresponding to the same parameters as the *in situ* images. We find a narrow condensed mode whose size remains roughly constant as the time of flight is increased and a wider thermal component that expands rapidly [43]. This allows us to define a condensed fraction as the ratio of minority atoms in the condensate mode to the total number of minority atoms. The paired nature of the condensate is confirmed by the observation that both the optical density and the width of the narrow mode match between majority and minority clouds.

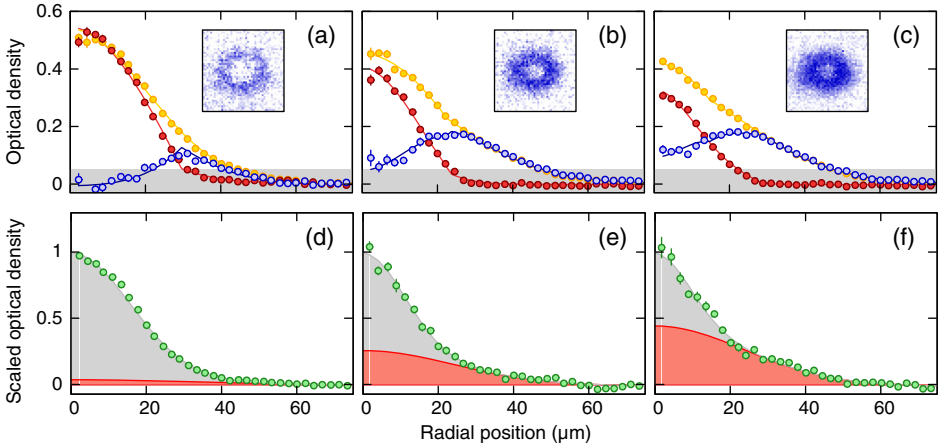

FIG. 2. Phase separation and condensation vs global polarization. (a)–(c) Azimuthal average of *in situ* OD of majority (yellow) and minority (red) clouds, and of their difference (blue) for $P = 0.25, 0.55$, and 0.75, respectively, taken at a field of 780 G, with fits to the sum of a Gaussian and a Thomas-Fermi profile. The insets show the corresponding two-dimensional OD difference. The gray shaded region represents the systematic error in the determination of OD differences. The radial position is measured along the minor axis of the elliptical contour lines used for azimuthal averaging. (d)–(f) OD of the minority cloud after 3 ms time of flight normalized to its peak value, with a double Gaussian fit to the data. The thermal component is shaded in red, while the condensate is shaded in gray. Error bars represent the standard deviation of the mean in evaluating the azimuthal average. All distributions represent an average of 30 experimental realizations.

We have studied the stability of the spin-balanced condensate to chemical potential imbalance across the BEC-BCS crossover. The chemical potential imbalance is scanned by changing the minority atom number and hence the global polarization P. The tight confinement of the gas along the axial direction allows for a two-body bound state with binding energy E_B even above the Feshbach resonance, unlike the 3D case. The absence of a unitarity point in the quasi-2D case makes the distinction between the BEC and BCS regimes more *ad hoc* than in three dimensions. We choose to characterize the interaction strength using the ratio E_B/E_F, where $E_F = \hbar\sqrt{2\omega_x\omega_y N_\uparrow}$ is the Fermi energy of the majority atoms in the non-interacting gas. We identify the BEC regime with $E_B/E_F \gg 1$ and the BCS regime with $E_B/E_F \ll 1$. The central polarization of the gas $p(0)$ is shown in Fig. 3 vs P for Feshbach fields of 730, 755, 780, 830, and 920 G. The respective values of E_B/E_F are ~6(1), 2.9(7), 1.4(3), 0.32(7), and 0.05(2). We find that $p(0)$ is consistent with zero within experimental uncertainty for a range of P less than a field-dependent critical polarization P_c. In the BEC regime, the gas may be thought of as an interacting Bose-Fermi mixture of deeply bound dimers and excess majority atoms, with strong atom-dimer repulsion leading to the observed profiles. This picture is supported by comparison of a mean field model with the data in the BEC regime [43]. In the BCS regime, the superfluid gap prevents fermionic quasiparticles from entering the superfluid below the Clogston limit. We find that P_c decreases as the BCS limit is approached as summarized in Fig. 4. Our observed critical polarization is consistent with a previous measurement [42] for comparable values of E_B/E_F.

We observe pair condensation that persists to high values of P at 730, 755, and 780 G [Figs. 3(a)–3(c)], even beyond P_c, pointing to a polarized condensate. For $B = 830$ and 920 G, no bimodality is observed. This can be anticipated for expansion in three dimensions since there is no bound state beyond the Feshbach resonance and the fragile dimers that exist in the trapped system break after release. The measured condensate fraction for a balanced gas is compatible with the fraction that has been measured recently [38] for comparable T/T_F^0. Similar to experiments in three dimensions [19], we find that the condensate fraction does not drop monotonically with increasing P as one would expect naively, but rather peaks at a nonzero P. The harmonic confinement of the clouds may explain this observation. Although the absolute temperatures we measure are independent of P [43], increasing P leads to a shrinking minority cloud whose wings experience a higher majority density, and therefore a higher local critical temperature.

Figure 5 shows an experimental phase diagram of a spin-imbalanced 2D Fermi gas for four different values of the interaction strength E_B/E_F. These phase diagrams show the local polarization $p(r)$ as a function of the global polarization P and the position in the trap r scaled by the Thomas-Fermi radius of a fully polarized gas $R_{\mathrm{TF}\uparrow}$, defined as $V(R_{\mathrm{TF}\uparrow}) = \mu_{0\uparrow}$ [43]. The global polarization P is the experimental parameter that determines the chemical potential difference $h = (\mu_\uparrow - \mu_\downarrow)/2$, while r fixes the average local chemical potential $\mu = (\mu_\uparrow + \mu_\downarrow)/2$, so we can interpret these diagrams as "$\mu - h$" phase diagrams expressed in terms of experimentally measured quantities. The partially polarized phase occupying the part of the phase diagram between the balanced condensate and the fully polarized normal gas, and depending on E_B/E_F, may be a Sarma phase induced by quantum or thermal fluctuations, an FFLO phase, or a Fermi liquid phase.

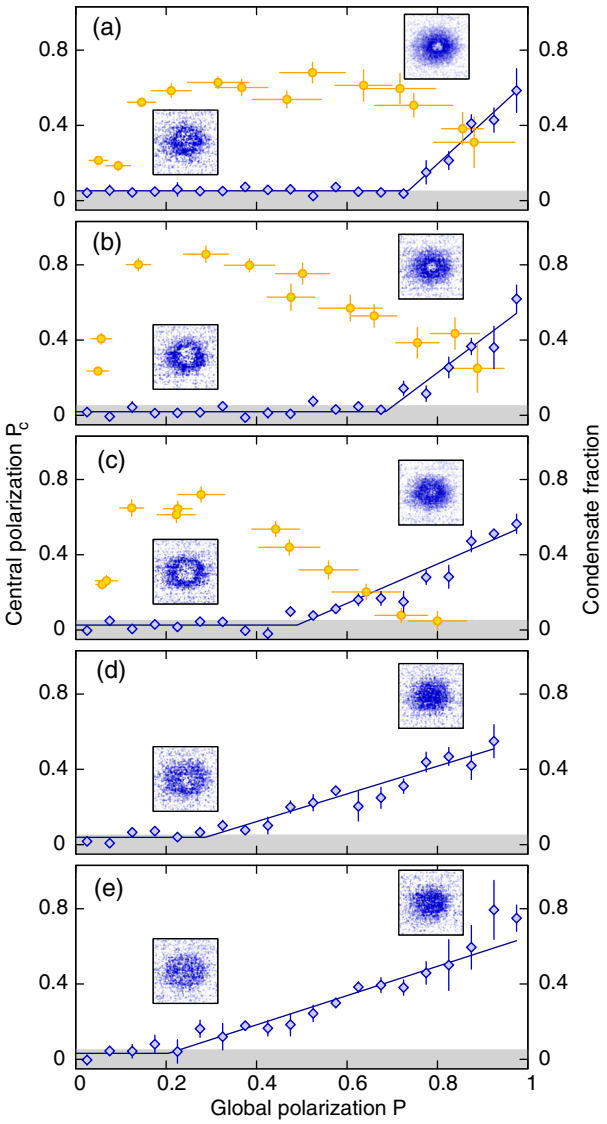

FIG. 3. Central polarization and condensate fraction vs global polarization. Central polarization (blue diamonds) and condensate fraction (yellow circles) are shown for the Feshbach fields of (a) 730, (b) 755, (c) 780, (d) 830, and (e) 920 G. The points represent the average of 5–15 experimental realizations, and error bars are the standard deviation of the mean. The gray region indicates the experimental uncertainty in the determination of the central polarization. The blue line is a bilinear fit to the data to determine P_c. For condensate fraction data, each point is obtained from a bootstrap analysis of 30 experimental shots. Error bars represent the standard deviation of the bootstrap distribution. The insets show the OD difference at $P = 0.25$ and 0.75.

Unlike the 3D case [23], we have not observed discontinuities in the polarization or density profiles. Zero temperature phase diagrams in Refs. [7,8,10] predict a first order phase transition between the superfluid and normal phases driven by the change in the average local chemical potential in the trap. This would be manifested by a sudden jump of the local polarization from zero in the superfluid to a finite

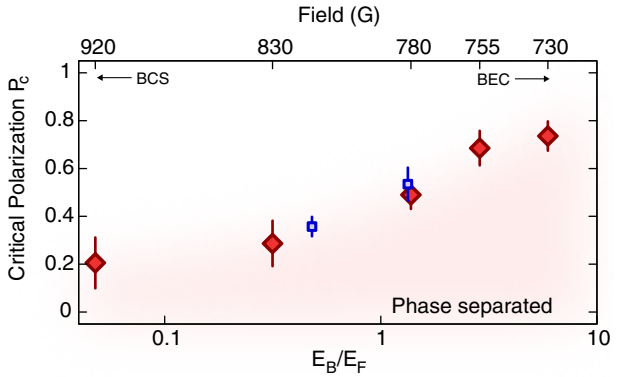

FIG. 4. Critical polarization (P_c) for phase separation vs E_B/E_F (log-scale). The global polarization at which phase separation ends is extracted from a bilinear fit to the central polarization data in Fig. 3 (red diamonds). Corresponding magnetic fields for these points are shown on the secondary x axis. For comparison, we extracted two points from the data of Ref. [42] (blue squares). The error bars are given by the fit uncertainty.

polarization in the normal phase. In three dimensions, the first order transition only occurs for temperatures below the tricritical point [50]. If such a tricritical point exists in two dimensions, it is possible that the temperature of our clouds is not low enough to observe the first order transition or that the one-dimensional nature of the interface between the superfluid and normal phases makes it very susceptible to fluctuations that smear out discontinuities when averaging over trap contour lines. We also note that strong quantum

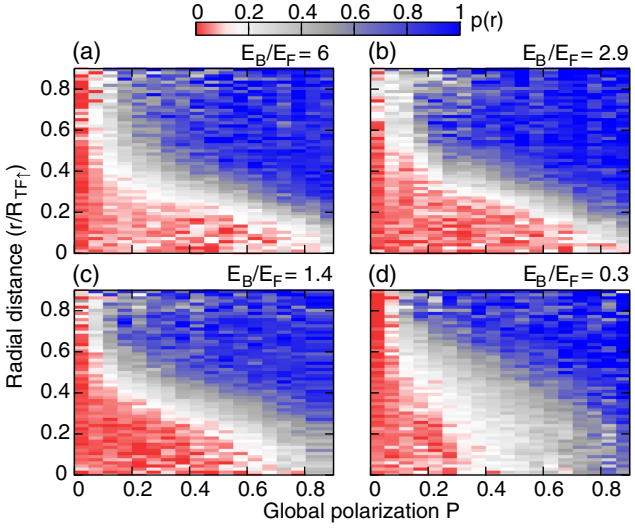

FIG. 5. Phase diagram of an imbalanced 2D Fermi gas for four different interactions determined by the Feshbach fields (a) 730, (b) 755, (c) 780, and (d) 830 G. The corresponding interaction strengths E_B/E_F are shown in the top-right corner of each panel. The color indicates the local polarization of the gas in the trap $p(r)$ as a function of the scaled position in the trap $r/R_{TF\uparrow}$ and the global polarization P. We distinguish three different phases: a balanced condensate (red), a partially polarized phase (white to gray), and a fully polarized normal gas (blue).

fluctuations in two dimensions can, in principle, drive the superfluid to normal transition continuous [12].

In conclusion, we have observed pair condensation in an imbalanced Fermi gas across the BEC-BCS crossover, accompanied by phase separation in the trap. In future work, it will be interesting to study the effect of thermal fluctuations on superfluidity in the imbalanced 2D gas and to determine if imbalance affects the BKT nature of the transition. Another interesting direction is the investigation of the partially polarized gas between the balanced condensate and the fully polarized normal gas. The partially polarized gas may host a variety of phases, including Sarma or FFLO states, whose stability is enhanced in lower dimensions.

We thank David Huse, Päivi Törmä, and Philipp Strack for useful discussions and Martin Zwierlein for critical reading of the manuscript. We thank John Thomas, Ilya Arakelyan, and co-workers for sharing their data. This work was supported by the NSF and the AFOSR Young Investigator Research Program. W. S. B. was supported by an Alfred P. Sloan Foundation fellowship and P. T. B. was supported by the DOD through the NDSEG Fellowship Program.

*debayan@princeton.edu

[1] A. M. Clogston, Phys. Rev. Lett. **9**, 266 (1962).
[2] G. Sarma, J. Phys. Chem. Solids **24**, 1029 (1963).
[3] P. Fulde and R. A. Ferrell, Phys. Rev. **135**, A550 (1964).
[4] A. I. Larkin and Yu. N. Ovchinnikov, Zh. Eksp. Teor. Fiz. **47**, 1136 (1964) [Sov. Phys. JETP **20**, 762 (1965)].
[5] M. M. Parish, S. K. Baur, E. J. Mueller, and D. A. Huse, Phys. Rev. Lett. **99**, 250403 (2007).
[6] T. K. Koponen, T. Paananen, J.-P. Martikainen, M. R. Bakhtiari, and P. Törmä, New J. Phys. **10**, 045014 (2008).
[7] G. J. Conduit, P. H. Conlon, and B. D. Simons, Phys. Rev. A **77**, 053617 (2008).
[8] L. He and P. Zhuang, Phys. Rev. A **78**, 033613 (2008).
[9] A. M. Fischer and M. M. Parish, Phys. Rev. B **90**, 214503 (2014).
[10] D. E. Sheehy, Phys. Rev. A **92**, 053631 (2015).
[11] S. Yin, J.-P. Martikainen, and P. Törmä, Phys. Rev. B **89**, 014507 (2014).
[12] P. Strack and P. Jakubczyk, Phys. Rev. X **4**, 021012 (2014).
[13] P. F. Bedaque, H. Caldas, and G. Rupak, Phys. Rev. Lett. **91**, 247002 (2003).
[14] J. Carlson and S. Reddy, Phys. Rev. Lett. **95**, 060401 (2005).
[15] D. E. Sheehy and L. Radzihovsky, Phys. Rev. Lett. **96**, 060401 (2006).
[16] D. E. Sheehy and L. Radzihovsky, Ann. Phys. (Amsterdam) **322**, 1790 (2007).
[17] C.-T. Wu, B. M. Anderson, R. Boyack, and K. Levin, arXiv:1605.01479.
[18] *The BCS-BEC Crossover and the Unitary Fermi Gas*, edited by W. Zwerger (Springer, Heidelberg, 2012).
[19] M. W. Zwierlein, A. Schirotzek, C. H. Schunck, and W. Ketterle, Science **311**, 492 (2006).
[20] Y. Shin, M. W. Zwierlein, C. H. Schunck, A. Schirotzek, and W. Ketterle, Phys. Rev. Lett. **97**, 030401 (2006).
[21] G. B. Partridge, W. Li, R. I. Kamar, Y. Liao, and R. G. Hulet, Science **311**, 503 (2006).
[22] M. W. Zwierlein, C. H. Schunck, A. Schirotzek, and W. Ketterle, Nature (London) **442**, 54 (2006).
[23] Y.-i. Shin, C. H. Schunck, A. Schirotzek, and W. Ketterle, Nature (London) **451**, 689 (2008).
[24] B. A. Olsen, M. C. Revelle, J. A. Fry, D. E. Sheehy, and R. G. Hulet, Phys. Rev. A **92**, 063616 (2015).
[25] N. Navon, S. Nascimbène, F. Chevy, and C. Salomon, Science **328**, 729 (2010).
[26] S. Nascimbène, N. Navon, K. J. Jiang, F. Chevy, and C. Salomon, Nature (London) **463**, 1057 (2010).
[27] Y. Liao, A. S. C. Rittner, T. Paprotta, W. Li, G. B. Partridge, R. G. Hulet, S. K. Baur, and E. J. Mueller, Nature (London) **467**, 567 (2010).
[28] K. Martiyanov, V. Makhalov, and A. Turlapov, Phys. Rev. Lett. **105**, 030404 (2010).
[29] B. Fröhlich, M. Feld, E. Vogt, M. Koschorreck, W. Zwerger, and M. Köhl, Phys. Rev. Lett. **106**, 105301 (2011).
[30] M. Feld, B. Fröhlich, E. Vogt, M. Koschorreck, and M. Köhl, Nature (London) **480**, 75 (2006).
[31] P. Dyke, E. D. Kuhnle, S. Whitlock, H. Hu, M. Mark, S. Hoinka, M. Lingham, P. Hannaford, and C. J. Vale, Phys. Rev. Lett. **106**, 105304 (2011).
[32] A. T. Sommer, L. W. Cheuk, M. J. H. Ku, W. S. Bakr, and M. W. Zwierlein, Phys. Rev. Lett. **108**, 045302 (2012).
[33] Y. Zhang, W. Ong, I. Arakelyan, and J. E. Thomas, Phys. Rev. Lett. **108**, 235302 (2012).
[34] V. Makhalov, K. Martiyanov, and A. Turlapov, Phys. Rev. Lett. **112**, 045301 (2014).
[35] I. Boettcher, L. Bayha, D. Kedar, P. A. Murthy, M. Neidig, M. G. Ries, A. N. Wenz, G. Zürn, S. Jochim, and T. Enss, Phys. Rev. Lett. **116**, 045303 (2016).
[36] K. Fenech, P. Dyke, T. Peppler, M. G. Lingham, S. Hoinka, H. Hu, and C. J. Vale, Phys. Rev. Lett. **116**, 045302 (2016).
[37] P. Dyke, K. Fenech, T. Peppler, M. G. Lingham, S. Hoinka, W. Zhang, S.-G. Peng, B. Mulkerin, H. Hu, X.-J. Liu, and C. J. Vale, Phys. Rev. A **93**, 011603 (2016).
[38] M. G. Ries, A. N. Wenz, G. Zürn, L. Bayha, I. Boettcher, D. Kedar, P. A. Murthy, M. Neidig, T. Lompe, and S. Jochim, Phys. Rev. Lett. **114**, 230401 (2015).
[39] P. A. Murthy, I. Boettcher, L. Bayha, M. Holzmann, D. Kedar, M. Neidig, M. G. Ries, A. N. Wenz, G. Zürn, and S. Jochim, Phys. Rev. Lett. **115**, 010401 (2015).
[40] C.-T. Wu, B. M. Anderson, R. Boyack, and K. Levin, Phys. Rev. Lett. **115**, 240401 (2015).
[41] M. Koschorreck, D. Pertot, E. Vogt, B. Fröhlich, M. Feld, and M. Köhl, Nature (London) **485**, 619 (2012).
[42] W. Ong, C. Cheng, I. Arakelyan, and J. E. Thomas, Phys. Rev. Lett. **114**, 110403 (2015).
[43] See Supplemental Material at http://link.aps.org/supplemental/10.1103/PhysRevLett.117.093601 for details on experiment and data analysis, which includes Refs. [44–49].

[44] H. P. Büchler and G. Blatter, Phys. Rev. A **69**, 063603 (2004).
[45] Y.-i. Shin, A. Schirotzek, C. H. Schunck, and W. Ketterle, Phys. Rev. Lett. **101**, 070404 (2008).
[46] G. V. Skorniakov and K. A. Ter-Martirosian, Zh. Eksp. Teor. Fiz. **31**, 775 (1957) [Sov. Phys. JETP **4**, 648 (1957)].
[47] D. S. Petrov, M. A. Baranov, and G. V. Shlyapnikov, Phys. Rev. A **67**, 031601 (2003).
[48] D. S. Petrov, C. Salomon, and G. V. Shlyapnikov, Phys. Rev. Lett. **93**, 090404 (2004).
[49] G. Zürn, T. Lompe, A. N. Wenz, S. Jochim, P. S. Julienne, and J. M. Hutson, Phys. Rev. Lett. **110**, 135301 (2013).
[50] M. M. Parish, F. M. Marchetti, A. Lamacraft, and B. D. Simons, Nat. Phys. **3**, 124 (2007).